IEEE Access
Multidisciplinary ⋮ Rapid Review ⋮ Open Access Journal

Received 1 March 2023, accepted 12 March 2023, date of publication 15 March 2023, date of current version 21 March 2023.

Digital Object Identifier 10.1109/ACCESS.2023.3257350

RESEARCH ARTICLE

A Tunable D-Band Filter Based on MOSCAP in 65nm CMOS Technology

SIROUS BAHRAMI, KANGSEOP LEE, (Student Member, IEEE), AND HO-JIN SONG, (Senior Member, IEEE)

Department of Electrical Engineering, Pohang University of Science and Technology, Pohang 37673, South Korea

Corresponding author: Sirous Bahrami (bahramis@postech.ac.kr)

This work was supported by the Institute of Information & communications Technology Planning & Evaluation (IITP) grant funded by the Korean Government [Ministry of Science and ICT (MSIT)] (No.2018-0-00823, Investigation on future mm-wave circuits, packages, and system).

ABSTRACT In this paper, a D-band varactor-based tunable bandpass filter is proposed in 65nm CMOS Technology. The filter is composed of coupled lines loaded with a pair of MOSCAPs that control the passband of the filter. The effects of MOSCAP parameters in terms of the quality factor and the tuning range are studied. The proper placement of the MOSCAP along the resonator is the key parameter to keep insertion loss as low as possible while the tuning range remains intact. A cross-coupled line between input/output ports introduces a pair of transmission zeros and significantly reduces the size of the filter. The tuning range of the proposed structure is 10 % (136 ∼ 150 GHz). For this frequency band, the fractional bandwidth (FBW) varies between 10.9 and 11.8 % and the in-band insertion loss is between 4 and 8.2 dB. The overall size of the filter is $0.11\lambda_0 \times 0.095\lambda_0$. Measurements for the filter show good agreement with the simulation results.

INDEX TERMS CMOS technology, mmwave technology, MOSCAP, TFMS, tunable bandpass filter.

I. INTRODUCTION

For mm-wave circuits application, it is sensible to provide a system-on-chip (SoC) solution, which permits passive and active components integration on the same substrate. This remarkably improves the system's reliability and reduces the cost of packaging [1]. A bandpass filter (BPF) is perhaps one of the most indispensable devices in RF circuits. Therefore, extensive methods have been presented recently in the design of on-chip BPFs using silicon-based [2] and III/V [3], [4], [5] technologies. Regarding on-chip filter design, several tradeoffs need to be considered to satisfy different design specifications, such as noise, bandwidth, linearity, die size, and insertion loss [6]. As the silicon substrate is inherently ''lossy'', the most effective method to minimize the insertion loss is to keep the design as compact as possible. Therefore, using a simple structure is preferred. Unlike the conventional distributed components usage for filter designs [7], [8], the quasi-lumped components approach has become popular lately [9], [10]. One of the main emerging approaches is to increase the self-coupling resonators by broadside coupling (metal stack-up) [11], [12]. Specifically, broadside-coupled meander-line resonator (BCMLR) based design has achieved very small dimensions [13], [14]. Since the vertical gap between metal layers is predefined and can not be changed planar structures with enhanced self-coupling are preferable [15], [16]. To improve the frequency selectivity and stopband suppression, one may introduce multiple transmission zeros (TZs) or appropriately adjust their positions [17]. In another approach, parasitic capacitances of a 3-D inductor were employed to generate an upper TZ [18]. Also, in [19] a capacitively loaded resonator is embedded in the original DGS resonator to form two high-quality (Q-) factor small loop resonators.

As the SoC solution applications push toward higher frequencies, demands for the on-chip BPF at higher spectrum such as D-band is also increasing. However, all of the previous works are up to E-band (<90 GHz). Moreover, despite the vast technical literature that can be found related to the fixed frequency on-chip filter, almost no efforts have been made regarding on-chip tunable BPF as RF-signal pre-selectors. As multi-channel systems are becoming more feasible,

The associate editor coordinating the review of this manuscript and approving it for publication was Harikrishnan Ramiah.

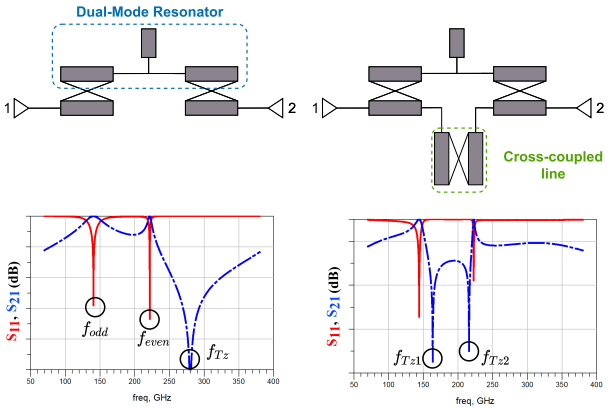

FIGURE 1. Dual-mode resonator with uncoupled even/odd modes and a pair of transmission zeros.

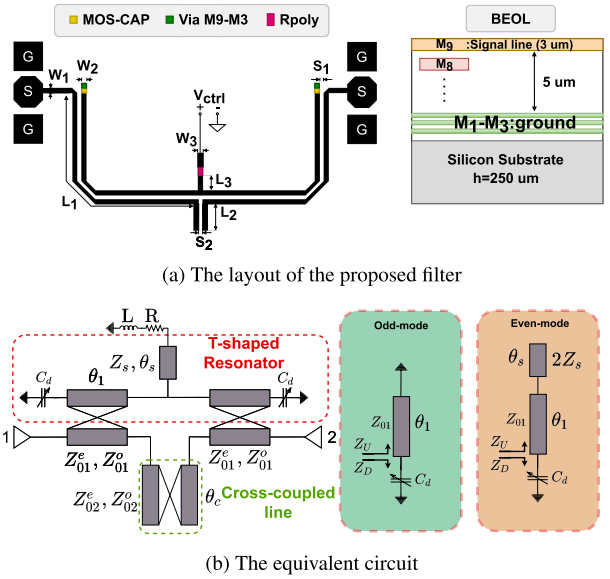

(a) The layout of the proposed filter

(b) The equivalent circuit

FIGURE 2. The proposed D-band CMOS tunable bandpass filter (a) structure ($L_1 = 203$um, $L_2 = 27.5$um, $L_3 = 5.5$um, $W_1 = W_2 = 5$um, $W_3 = 2$um, $S_1 = 4$um, $S_2 = 2$um.), (b) equivalent-circuit model (the DC bias line is indicated with a resistor R and an inductance L) and even/odd modes.

tunable BPFs are becoming more attractive in modern communication applications [20], [21], [22], [23], [24], [25]. Although few tunable BPFs at mm-wave bands are reported in different technologies [26], [27], [28], [29], [30], [31], [32], their on-chip implementation has not been reported yet. One of the main bottlenecks regarding the feasibility of on-chip tunable filters, especially at the mm-wave band, is the reduced Q-factor of the varactors at higher frequencies [33]. In this paper, we investigate the feasibility of a MOSCAP-based tunable BPF at the D-band frequency range for the first time. The proposed on-chip filter structure consists of a T-shaped resonator and a cross-coupled line. The cross-coupled line not only reduces the size of the filter but also increases the selectivity of the filter by introducing a pair of upper TZs. A pair of MOSCAPs with a single bias line is employed to tune the passband of the filter. The effects of MOSCAP parameters on the insertion loss, Q-factor, and tuning range of the proposed BPF are studied. Although MOSCAPs show a very low Q-factor at high frequencies, it is shown that their proper placement within the filter structure can substantially compensate for the insertion loss. The priority of this filter design is to achieve a higher tuning range and a lower insertion loss.

This paper is organized as follows. The design procedure of the basic BPF is provided in section II. In section III the extensive study of MOSCAP is presented. The large signal analysis of the proposed BPF is studied for different MOSCAP configurations in section IV. Simulation and measurement results of the proposed tunable filter are presented in section V. Next, the performance of the proposed BPF is compared with previous works in section VI. Finally, conclusions are drawn in Section VII.

II. DESIGN OF THE TUNABLE ON-CHIP BPF

A. CLASSIFICATION OF DUAL-MODE RESONATORS

Dual-mode resonators are categorized by having coupled or uncoupled even/odd modes [34]. Coupled dual-mode resonators with two close transmission poles (f_{odd} and f_{even}) are extensively used as the core of BPF structures. These types of resonators yield a limited tuning range with insufficient selectivity since the spacing between transmission poles increases in the lower bound of the tuning range. To alleviate this issue, we are particularly interested in the uncoupled resonator where a wide gap exists between f_{odd} and f_{even}. As mentioned in [34], for these types of resonators, there is an intrinsic transmission zero at the high side of f_{odd} and f_{even} (Fig. 1(a)). Interestingly, by inserting an input/output cross-coupling one can generate a pair of TZs (f_{TZ1} and f_{TZ2}) between f_{odd} and f_{even} as shown in Fig. 1(b). Therefore, the key idea in the proposed BPF is that by adjusting the lower Transmission zero f_{TZ1} near f_{odd} we can increase the selectivity. More details about the operation of the proposed BPF are provided in the following subsections.

B. T-SHAPED RESONATOR

Fig. 2 shows the proposed tunable bandpass filter. The SiO_2 substrate parameters are $\varepsilon_r = 3.9$, $\tan\delta = 0.002$. The T-shaped resonator consists of an open stub (Z_s, θ_s) and two coupled lines loaded with a pair of MOSCAPs. Another coupled line is introduced in the middle of the main signal path to form a cross-coupling between the input and the output. The DC biasing of the MOSCAPs is inserted at the edge of the open stub with a resistor R and an inductance L. The equivalent circuit of the filter is illustrated in Fig. 2(b). The impedance of the series RL for DC blockage is high enough to be considered an open circuit for even mode analysis.

The varactor-loaded T-shaped resonator is responsible for tuning the filter's passband. The structure is symmetrical and one can apply even-odd mode analysis. This resonator's even- and odd-mode equivalent circuits are depicted in Fig. 2(b). For the desired tunable resonant frequencies of the even/odd

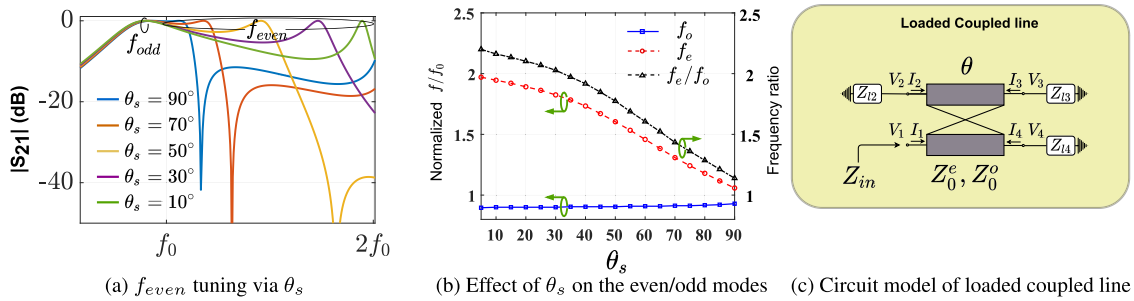

(a) f_{even} tuning via θ_s (b) Effect of θ_s on the even/odd modes (c) Circuit model of loaded coupled line

FIGURE 3. The frequency response (a) for different values of the electrical length θ_s, (b) f_{even}, f_{odd} against θ_s, (c) a loaded coupled-line.

modes, the impedances Z_U and Z_D in Fig. 2(b) must satisfy $Z_U + Z_D = 0$. Hence,

$$\frac{1}{\omega_{even} C_d} = \frac{2Z_{01}Z_s \cot\theta_s - Z_{01}^2 \tan\theta_1}{Z_{01} + 2Z_s \tan\theta_1 \cot\theta_s} \tag{1}$$

$$\frac{1}{\omega_{odd} C_d} = Z_{01} \tan\theta_1 \tag{2}$$

where $Z_{01} = \sqrt{Z_{01}^e Z_{01}^o}$ is the impedance of each arm of the T-shaped resonator and C_d is an ideal variable capacitance. In this design, we set the passband frequency on the lower transmission pole

$$f_{odd} = \frac{Y_{01}}{2\pi C_d} \cot\theta_1 \tag{3}$$

Based on (3), by changing the capacitance of the varactor C_d the central frequency of the BPF can be tuned. However, the other resonance that occurs at f_{even} must be located far beyond the passband of the BPF (i.e. $f_{even}/f_{odd} > 1$). According to (1), to shift the f_{even} to higher frequencies one plausible option is to adjust the electrical length of the central open-ended stub (i.e. θ_s). Fig. 3(a-b) show that decreasing the electrical length θ_s shifts the f_{even} to higher frequencies while f_{odd} remains constant. It is notable that in the case of $\theta_s = 90°$ the central stub line converts to a short-circuited transmission line and the structure becomes a conventional BPF. Thus, to keep $f_{even}/f_{odd} \geq 2$ one should restrict $\theta_s \leq 30°$.

C. CROSS-COUPLED LINE

The other important section of the filter structure is the middle coupled line which introduces a pair of transmission zeros beyond f_{odd} to increase the selectivity of the proposed filter. These transmission zeros can be calculated analytically as follows. First, the even- and odd-mode input impedances shown in Fig. 3(c) can be determined as

$$\begin{aligned} Z_{in}^e &= Z_{in}\big|_{Z_{l2}=\frac{1}{j\omega C_d}, Z_{l3}=-2jZ_s \cot\theta_s, Z_{l4}=-jZ_{02}^e \cot\theta_t} \\ Z_{in}^o &= Z_{in}\big|_{Z_{l2}=\frac{1}{j\omega C_d}, Z_{l3}=0, Z_{l4}=-jZ_{02}^o \cot\theta_t} \end{aligned} \tag{4}$$

where

$$Z_{1,2} = -j\frac{Z_0^e \pm Z_0^e}{2\tan\theta} \tag{5}$$

$$Z_{3,4} = -j\frac{Z_0^e \mp Z_0^e}{2\sin\theta}. \tag{6}$$

The Z_0^e and Z_0^o represent the even- and odd-mode impedances of the coupled lines, respectively. Next, the S-parameters of the tunable filter can be evaluated as

$$S_{21} = \frac{Z_0(Z_{in}^e - Z_{in}^o)}{(Z_0 + Z_{in}^e)(Z_0 + Z_{in}^o)} \tag{7}$$

$$S_{11} = \frac{Z_{in}^e Z_{in}^o - Z_0^2}{(Z_0 + Z_{in}^e)(Z_0 + Z_{in}^o)} \tag{8}$$

A pair of transmission zeros f_{z1} and f_{z2} are the solutions of $|S_{21}(f_{zi})| = 0$, and according to (8),

$$Z_{in}^e(f_{zi}) = Z_{in}^o(f_{zi}) \quad \text{for} \quad i = 1, 2 \tag{9}$$

The electrical size and the coupling factor of the cross-coupled line dictate the location and depth of these transmission zeros. As conceptually shown in Fig. 4(a), these frequencies can be tuned for a desirable selectivity and stopband ($|S_{21}| \leq -20$dB). If f_{z1} moves toward the passband edge frequency, higher selectivity will be achieved and a wide stopband is possible if the transmission zeros spacing grows. One parameter to indicate the selectivity of the BPF is the Roll-of-Rate (RoR) which is defined as

$$RoR\left(\frac{dB}{GHz}\right) = \frac{\alpha_{max} - \alpha_{min}}{f_c - f_s} \tag{10}$$

where, $\alpha_{max} = -40$dB is the stopband attenuation, $\alpha_{min} = -3$dB is the passband attenuation, f_c and f_s are the corresponding passband and stopband edge frequencies, respectively (Fig. 4(a)). Based on (7) and (10), the coupling factor ($\mathbf{k_c} = (Z_i^e - Z_i^o)/(Z_i^e + Z_i^o)$) and the electrical length (θ_c) of the middle coupled line can be used to control f_{z1}, f_{z2}. The simulation results in Fig. 4(b-d) illustrate the effect of the coupled line on the transmission zeros. According to Fig. 4(b), for the electrical length $\theta_c = 40°$ the stopband reaches the maximum of 88 GHz while for $\theta_c = 50°$ the RoR peaks at 2.9 ($\frac{dB}{GHz}$). These results can be well explained based on Fig. 4(c) where f_{z1} reaches its minimum at $\theta_c = 50°$.

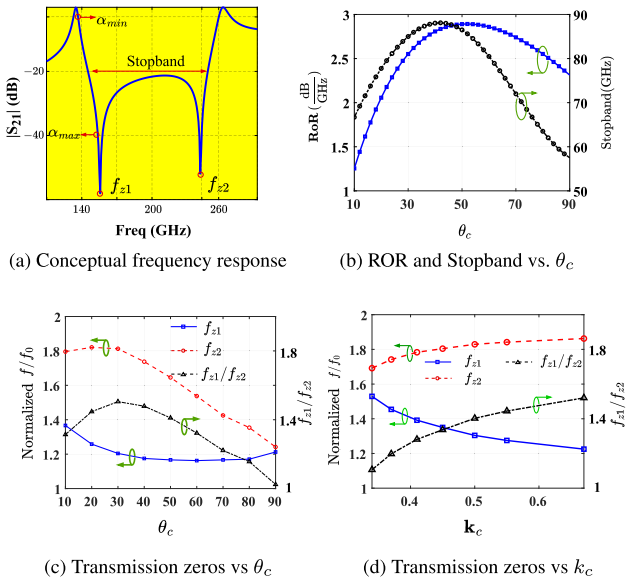

(a) Conceptual frequency response (b) ROR and Stopband vs. θ_c

(c) Transmission zeros vs θ_c (d) Transmission zeros vs k_c

FIGURE 4. **The RoR and Stopband (a) the graphical definition, (b) simulation results for different θ_c values. Transmission zeros against (c) the electrical length θ_c, (d) the coupling factor $\mathbf{k_c}$ (Z_{02}=41Ω).**

TABLE 1. **Parameters of the selected MOSCAPs.**

	WR(um)	LR (um)	GP	BR	FoM	$\mathbf{FoM_2}$	C(fF)
C_{I}	0.8	0.2	1	4	4.24	24.14	4.464
C_{II}	0.8	0.2	2	4	3.88	15.53	7.950
C_{III}	0.8	0.2	1	8	3.87	24.38	8.923
C_{IV}	0.8	0.6	1	4	3.79	23.32	7.532
C_{V}	0.4	0.2	1	4	3.29	17.64	3.238

Fig. 4(d) shows that f_{z1} constantly decreases for higher $\mathbf{k_c}$ values. In contrast, f_{z2} and consequently f_{z2}/f_{z1} increase by $\mathbf{k_c}$.

The next step is the proper selection of MOSCAP. It is worth noting that varactors with smaller capacitance will result in a wider tuning range. Based on (3), for the D-band frequency range, a MOSCAP in the order of 2 fF to 20 fF would be sufficient. Fig. 5(a) shows the simulation results for the equivalent circuit model of the proposed filter where the MOSCAP is replaced by an ideal capacitor. The filter tuning range spans from 130 GHz to 160 GHz. The coupled lines of the T-shaped resonator parameters are Z_{01}^{e}=66Ω, Z_{01}^{o}=45Ω and $\theta_1 = 55°$. The cross-coupling is responsible for upper-band transmission zero which significantly reduces the overall size of the filter. In Fig. 5(b) the external Q-factor for different spacing S_1 is shown. The Q-factor steadily increases with respect to S_1. In the next section, we delve deeper into the MOSCAP parameters to be exploited in the filter design.

III. MOSCAP ANALYSIS AND UTILIZATION

In this section, we investigate the topological parameters of the MOSCAP to tailor the BPF response based on the desired tuning range and insertion loss. The MOSCAP as shown in Fig. 6(a), has four topological parameters: unit cell width (WR) and length (LR), array size group number (GP), and branch number (BR). Since the priority is given to a wide

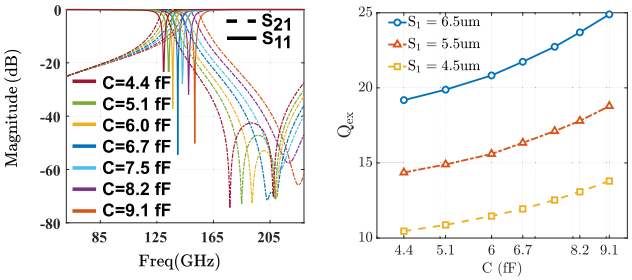

(a) Frequency response (b) Q_{ex} vs. resonator spacing

FIGURE 5. **Frequency response of the proposed filter (a) for different capacitance values C_d, (b) Q_{ex} for difference spacing S_1 and C_d values.**

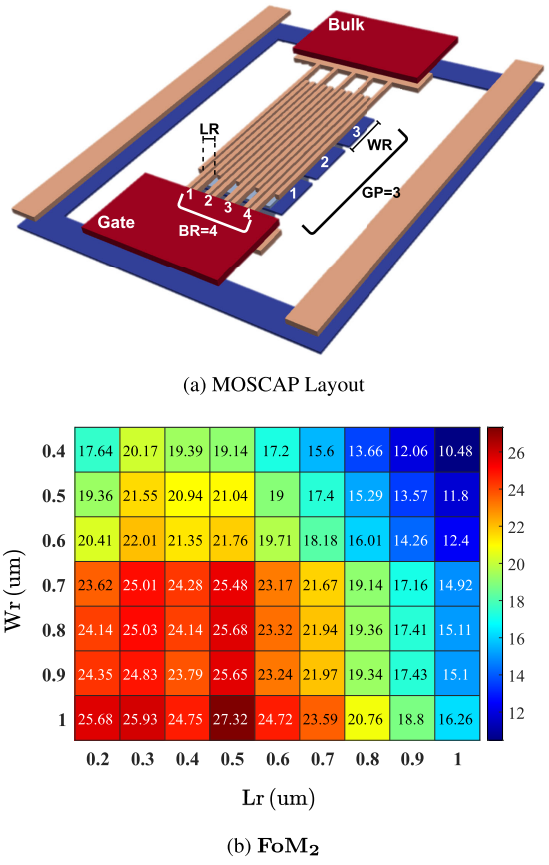

(a) MOSCAP Layout

(b) $\mathbf{FoM_2}$

FIGURE 6. **MOSCAP in 65nm Technology (a) 3D layout.$\mathbf{FoM_2}$ chart for parameters WR and LR (BR=4 and GP=1).**

tuning range and a low insertion loss one may define a figure-of-merit to indicate the overall performance of a tunable BPF as:

$$FoM = \frac{TR(\%)}{\overline{IL}(dB)} \tag{11}$$

where TR is the percentage of the tuning range and $\overline{\mathbf{IL}}$ is the average insertion loss over the tuning range. However primarily, we have to evaluate the parameters of the varactors independently. With this aim in view, another figure of merit is defined in [9] to evaluate the performance of a varactor

TABLE 2. Comparison of the proposed filter with some published mm-wave tunable structures.

Refs.	Frequency band (GHz)	Technology	Insertion Loss (dB)	Tuning range	FBW	FoM	Size (mm^2)
[27]	60	Liquid crystal	4.9–6.2	3 %	1 %	0.54	89.7×10^{-3}
[28]	78.5	MEMS	6.7	switchable	10-19.2 %	–	17.81
[29]	65	MEMS	1.5-5	6 %	3.4-8.3 %	1.84	2.5
[35]	56-74	MEMS	6.2-9.9	switchable	8.3-10.9 %	–	1.82
[36]	63	MEMS	2.9-4.8	4.8 %	4.5-5 %	1.04	96
[37]	50	Ferroelectric	4.9-7.6	8 %	8.7-9.7 %	1.63	3
This work	**140**	**MOSCAP**	**4.0-8.1**	**10 %**	**10.9-11.8 %**	**1.67**	**48.8×10^{-3}**

FBW: Fractional Bandwidth **FoM**=Tuning range (%) /IL (dB)

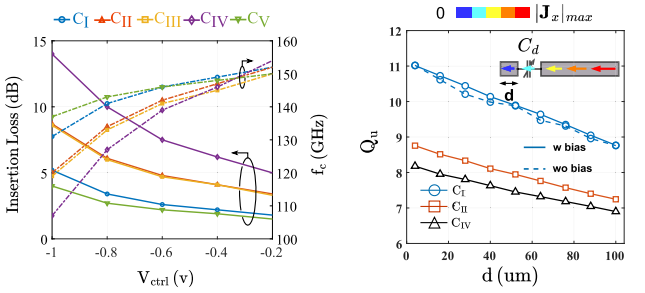

(a) IL and tuning range vs. biasing (b) Q_u vs. MOSCAP placement

FIGURE 7. The simulation results (a) insertion loss and the central frequency vs. control voltage for MOSCAPs listed in Table 1, (b) Q_u versus MOSCAP placement within the resonator for C_I (with/without the biasing network), C_{II} and C_{IV}.

which reads:

$$FoM_2 = Q\frac{C_{max}}{C_{min}} \tag{12}$$

where $\mathbf{C_{max}}$ and $\mathbf{C_{min}}$ are the maximum and minimum capacitance values of the varactor, respectively. The values of $\mathbf{FOM_2}$ are given based on topological parameters WR and LR in the chart of Fig. 6(b). Five potential MOSCAPs listed in Table 1 are investigated accordingly and they were compared based on their **FoM** values in the proposed BPF. In this stage, we should determine the performances of these MOSCAPs within the BPF structure. These MOSCAPs' performances in the proposed BPF are compared in Fig. 7(a). It can be seen that the C_{IV} has the highest insertion loss and tuning range. In contrast, C_V has the lowest insertion loss and tuning range. To maintain the insertion loss below 5 dB and achieve an acceptable tuning range C_I with WR = 0.8 um, LR = 0.2 um, GR = 1, and BR = 4 is the best configuration. Based on these observations, for the proposed tunable BPF design we can translate the desirable MOSCAP to have $\mathbf{FoM_2} \geq 24$ and $\mathbf{C_{min}} \leq 6$ fF.

It is important to highlight the fact that one of the design considerations is the proper placement of the varactors along the resonator to keep insertion loss as low as possible. From Fig. 7(b) it is evident that placing the varactor at the edge of the resonator yields the highest unloaded quality factor. since the current distribution decreases near the open end so less power would be lost in any edge-loaded MOSCAP. Furthermore, the Q-factor with/without the biasing is also depicted in Fig. 7(b). Since the passband is associated with the odd mode of the resonator, the biasing point at the central point of the resonator is a virtual ground, hence, the biasing effect on the Q-factor is negligible. The Q-factor and $\mathbf{FoM_2}$ of the selected MOSCAP are depicted in Fig. 8(a). The $\mathbf{FoM_2}$ values decrease over the bias tuning. At higher frequencies, $\mathbf{FoM_2}$ reduces even more due to Q-factor decline.

The capacitance value of C_I versus the control voltage is shown in Fig. 8(b). Around zero biasing voltage, the capacitance variation is small. However, near -1 V (shaded in pink in Fig. 8(b)) the capacitance decreases more sharply. Regarding the voltage control accuracy, by looking at (3) one can conclude that the sensitivity of the passband frequency is

$$\frac{\partial f_{odd}}{f_{odd}} = -\frac{\partial C_d}{C_d} \tag{13}$$

Hence, the frequency variations are higher for smaller capacitance values. Considering the average FBW of 11 % over the tuning range, its half value i.e., 5.5 % is acceptable for the capacitance variations. By utilizing Fig. 8(b), one can easily get the acceptable control voltage tolerance for the high selectivity of the proposed BPF. In the left side region of the plot, where $\mathbf{V_{ctrl}} > -0.8$ V, the voltage tolerance of 130 mV is acceptable. Although, in the shaded region of the plot, the acceptable voltage tolerance is merely 30 mV.

Based on the analysis given in Sections II and III, the design procedure of the proposed tunable BPF is as follows:

1) Select the initial electrical length of the T-shaped resonator (θ_1) at the fundamental passband frequency based on (3).
2) Select the electrical length of the open stub (θ_s) based on Fig. 3(b) for optimum frequency ratio f_{even}/f_{odd}.
3) Optimize the electrical length (θ_c) and the coupling factor (k_c) of the cross-coupling coupled line for the specified RoR and stopband.
4) Select the topological parameters of the MOSCAP for the trade-off between the tuning range and the insertion loss as exemplified in Fig. 7(a).

IV. LARGE SIGNAL ANALYSIS

For nonlinear characterization of the proposed filter the 1-dB compression point (P1 dB) and the third-order intercept point (IIP3) are extracted. A two-tone test with 200 MHz frequency spacing was used to analyze the filter with three MOSCAP configurations $\mathbf{C_I}$, $\mathbf{C_{II}}$, and $\mathbf{C_V}$. The simulation results of

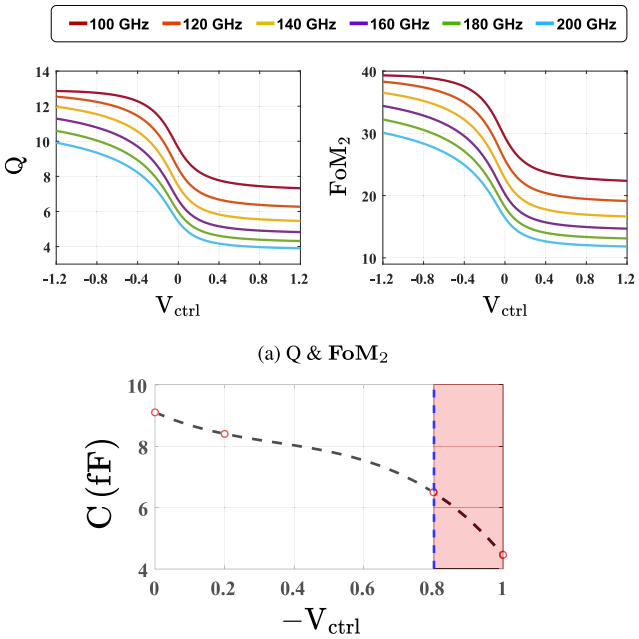

(a) Q & FoM_2

(b) Capacitance

FIGURE 8. The MOSCAP C_I, (a) the Q-factor and FoM_2, (b) capacitance versus the control voltage.

nonlinear performance are demonstrated in Fig. 9 (a-c). For the state-of-the-art RF, front end the performance of the proposed BPF is satisfactory in terms of linearity. The chosen MOSCAP $\mathbf{C_I}$ has an intermediate IM3 value in comparison to $\mathbf{C_{II}}$ and $\mathbf{C_V}$. Also, the noise figure of the filter with $\mathbf{C_I}$ and $\mathbf{C_{II}}$ is plotted against different biasing voltages in Fig. 9(d). Zero voltage biasing has the worst noise figure and $\mathbf{C_{II}}$ has better noise performance over the tuning range. These results imply that there is a trade-off between the tuning range, insertion loss, linearity, and noise figure of the tunable filter based on the MOSCAP selection. Therefore, one should select a proper MOSCAP configuration based on the required performance of the tunable filter.

V. MEASUREMENT SETUP

The proposed tunable BPF shown in Fig. 10 (a) was fabricated on 65nm TSMC CMOS technology. The overall size of the structure including the GSG and biasing pads is 0.5mm×0.7mm. The filter structure is formed on the M9 layer and M3 to M1 layers are grouped to form the ground plane. Two MOSCAPs are placed at two corner sides of the coupled line resonators and biased at the center via a rpoly resistor R=1 kΩ and a high impedance line.

The measurement setup is illustrated in Fig. 10 (b). An N5247B PNA-X Microwave Network Analyzer and a pair of VDI WR 6.5 extenders (110-170 GHz) were used for measurements. In four measuring states, the control voltage was set to −1, −0.8, −0.2, and 0 V to change the capacitance of MOSCAPs. In each voltage state, the S-parameters of the filter are recorded over the frequency range.

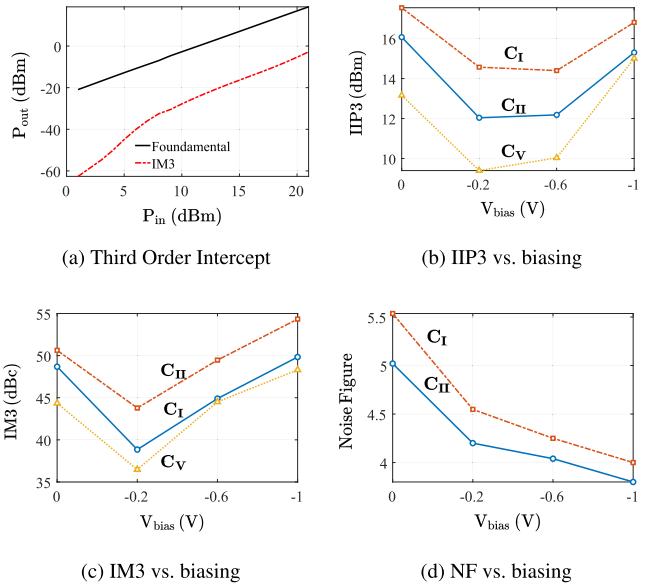

(a) Third Order Intercept (b) IIP3 vs. biasing

(c) IM3 vs. biasing (d) NF vs. biasing

FIGURE 9. Nonlinear and Noise analysis of the filter. (a) Third order intercept of C_I for $V_{bias} = -0.2$V, (b) IIP3 versus V_{bias} for three MOSCAPs, (c) IM3 versus V_{bias}. (d) Noise Figure versus V_{bias}.

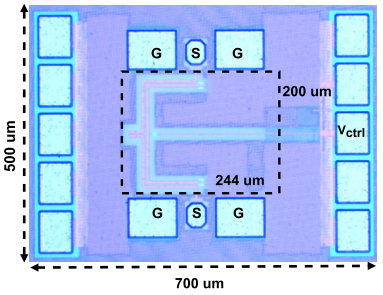

(a) Fabricated BPF

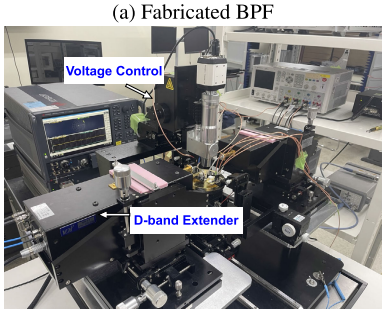

(b) Measurement setup

FIGURE 10. (a) The fabricated tunable BPF and (b) the measurement setup.

VI. RESULTS AND DISCUSSION

The measurement results for S-parameters after de-embedding pad parasitic components are depicted in Fig. 11(a,b). The tuning range of the proposed filter is from 136 GHz to 150 GHz and the insertion loss varies from −4.0 dB to −8.2 dB. The reflection coefficient varies between 18 and 10 dB. Also, fig. 11 (c) shows the group delay (GD) for different tuning states. The proposed filter has a narrow bandwidth and comparatively higher GD is expected around the passband.

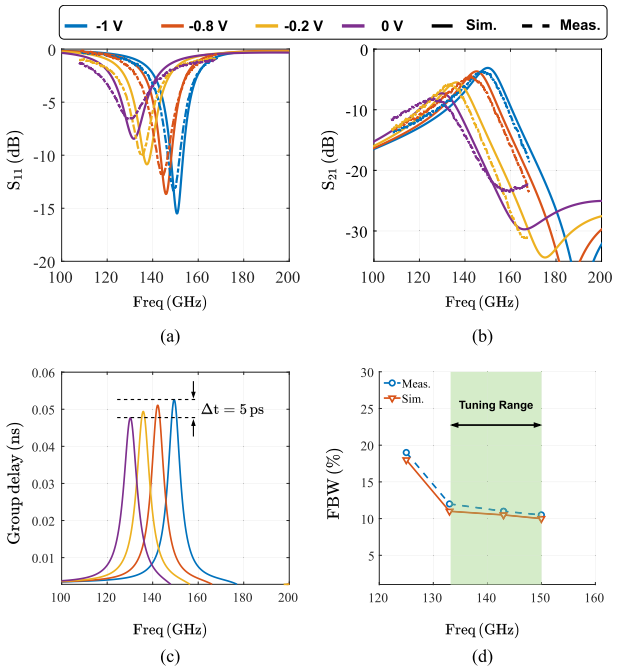

FIGURE 11. The simulation and measurement results for the proposed BPF (a) the reflection coefficient, (b) the transmission coefficient, (c) group delay, (d) FBW.

TABLE 3. Comparison with some previous on-chip BPFs.

Reference	f_0 (GHz)	FBW (%)	IL (dB)	Size (mm^2)	Tunability	Technology
[3]	60	18.4	2.42	0.054	×	0.15-μm GaAs
[5]	67.5	35.3	1.7	0.585	×	0.15-μm GaAs
[7]	58	27	4	0.1845	×	0.18-μm CMOS
[8]	60	30	2.5	0.15	×	0.18-μm CMOS
[11]	35	21.9	1.7	0.039	×	0.13-μm CMOS
[13]	33	42.4	2.6	0.03	×	0.13-μm CMOS
[17]	33	66.7	1.5	0.07	×	45nm CMOS
This Work	**140**	**11.4**	**4-8.1**	**0.049**	✓	**65nm CMOS**

The important factor is the consistency of GD over the tuning range. The GD values are between 48 to 53 ps over the tuning range, hence GD variation Δt is 5 ps which is acceptable at the D-band frequency range. Also, the fractional bandwidth (FBW) of the proposed BPF in four tuning states is illustrated in Fig. 11(d). The FBW is between 10.9 and 11.8%. Measurement results show good agreement with the simulation results. As the passband shifts to lower frequencies, the insertion loss increases while the Q-factor decreases from 10 at 150 GHz to 5 at 125 GHz. This phenomenon restricts the tuning range and is attributed to the parameters of the MOSCAP as explained in section III. The proposed BPF is compared with other tunable filters in Table 2. Although the proposed tunable filter is implemented on-chip and operates at higher frequencies, its performance in terms of the tuning range and FoM is comparable with previous works. Furthermore, the proposed filter is compared with some previous mm-wave on-chip BPF in Table 3. Frequency tuning gives the proposed on-chip filter an edge over its fixed counterparts. Relatively higher insertion loss of the proposed BPF is attributed to the low Q factor of MOSCAPs and greater metal loss at higher frequencies.

VII. CONCLUSION

In this paper, a tunable BPF is designed and fabricated on 65nm CMOS technology at the D-band frequency range for the first time. A pair of MOSCAPs is employed to control the passband of the filter. A tuning range of 14 GHz was measured, which corresponds to a tunability of 10 %. The minimum measured insertion loss is −4.0 dB and the FBW changes from 10.9% to 11.8%. This work serves as an initial study of D-band tunable filters in CMOS technology. The study of topological parameters of MOSCAP shows that there is a trade-off between the tuning range, insertion loss, linearity, and noise figure of the tunable filter. Therefore, one should select a proper MOSCAP configuration based on the required performance of the tunable filter.

REFERENCES

[1] S. Chakraborty, Y. Yang, X. Zhu, O. Sevimli, Q. Xue, K. Esselle, and M. Heimlich, "A broadside-coupled meander-line resonator in 0.13-μm SiGe technology for millimeter-wave application," *IEEE Electron Device Lett.*, vol. 37, no. 3, pp. 329–332, Mar. 2016.

[2] K.-D. Xu, X. Zhu, Y. Yang, and Q. Chen, "A broadband on-chip bandpass filter using shunt dual-layer meander-line resonators," *IEEE Electron Device Lett.*, vol. 41, no. 11, pp. 1617–1620, Nov. 2020.

[3] K.-D. Xu, Y.-J. Guo, Y. Liu, X. Deng, Q. Chen, and Z. Ma, "60-GHz compact dual-mode on-chip bandpass filter using GaAs technology," *IEEE Electron Device Lett.*, vol. 42, no. 8, pp. 1120–1123, Aug. 2021.

[4] Y.-P. Lyu, Y.-J. Zhou, L. Zhu, and C.-H. Cheng, "Compact and high-order on-chip wideband bandpass filters on multimode resonator in integrated passive device technology," *IEEE Electron Device Lett.*, vol. 43, no. 2, pp. 196–199, Feb. 2022.

[5] Y.-J. Guo, K.-D. Xu, X. Deng, X. Cheng, and Q. Chen, "Millimeter-wave on-chip bandpass filter based on spoof surface plasmon polaritons," *IEEE Electron Device Lett.*, vol. 41, no. 8, pp. 1165–1168, Aug. 2020.

[6] Y. Zhong, Y. Yang, X. Zhu, E. Dutkiewicz, K. M. Shum, and Q. Xue, "An on-chip bandpass filter using a broadside-coupled meander line resonator with a defected-ground structure," *IEEE Electron Device Lett.*, vol. 38, no. 5, pp. 626–629, May 2017.

[7] K. Ma, S. Mou, and K. S. Yeo, "Miniaturized 60-GHz on-chip multimode quasi-elliptical bandpass filter," *IEEE Electron. Devices Lett.*, vol. 34, no. 8, pp. 945–947, Aug. 2013.

[8] N. Mahmoud, A. Barakat, A. B. Abdel-Rahman, A. Allam, and R. K. Pokharel, "Compact size on-chip 60 GHz H-shaped resonator BPF," *IEEE Microw. Wireless Compon. Lett.*, vol. 26, no. 9, pp. 681–683, Sep. 2016.

[9] F. Sun, H. Zhu, X. Zhu, Y. Yang, and R. Gómez-García, "Design of on-chip millimeter-wave bandpass filters using multilayer patterned-ground element in 0.13-μm (Bi)-CMOS technology," *IEEE Trans. Microw. Theory Techn.*, vol. 67, no. 12, pp. 5159–5170, Dec. 2019.

[10] Z. J. Hou, Y. Yang, X. Zhu, Y. C. Li, E. Dutkiewicz, and Q. Xue, "A compact and low-loss bandpass filter using self-coupled folded-line resonator with capacitive feeding technique," *IEEE Electron Device Lett.*, vol. 39, no. 10, pp. 1584–1587, Oct. 2018.

[11] Y. Yang, H. Zhu, X. Zhu, and Q. Xue, "A low-loss bandpass filter using edge-coupled resonator with capacitive feeding in (Bi)-CMOS technology," *IEEE Electron Device Lett.*, vol. 39, no. 6, pp. 787–790, Jun. 2018.

[12] H. Zhu, X. Zhu, Y. Yang, and Y. Sun, "Design of miniaturized on-chip bandpass filters using inverting-coupled inductors in (Bi)-CMOS technology," *IEEE Trans. Circuits Syst. I, Reg. Papers*, vol. 67, no. 2, pp. 647–657, Feb. 2020.

[13] Y. Yang, H. Liu, Z. J. Hou, X. Zhu, E. Dutkiewicz, and Q. Xue, "Compact on-chip bandpass filter with improved in-band flatness and stopband attenuation in 0.13-μm (Bi)-CMOS technology," *IEEE Electron Device Lett.*, vol. 38, no. 10, pp. 1359–1362, Oct. 2017.

[14] L. Chen, H. Zhu, R. Gomez-Garcia, and X. Zhu, "Miniaturized on-chip notch filter with sharp selectivity and >35-dB attenuation in 0.13-μm bulk CMOS technology," *IEEE Electron Device Lett.*, vol. 43, no. 8, pp. 1175–1178, Aug. 2022.

[15] M. G. Bautista, H. Zhu, X. Zhu, Y. Yang, Y. Sun, and E. Dutkiewicz, "Compact millimeter-wave bandpass filters using quasi-lumped elements in 0.13-μm (Bi)-CMOS technology for 5G wireless systems," *IEEE Trans. Microw. Theory Techn.*, vol. 67, no. 7, pp. 3064–3073, Jul. 2019.
[16] V. N. R. Vanukuru and V. K. Velidi, "CMOS millimeter-wave ultra-wideband bandpass filter with three reflection-zeros using compact single TFMS coupled-line hairpin unit," *IEEE Trans. Circuits Syst. II, Exp. Briefs*, vol. 67, no. 1, pp. 77–81, Jan. 2020.
[17] L. Gao and G. M. Rebeiz, "Wideband bandpass filter for 5G millimeter-wave application in 45-nm CMOS silicon-on-insulator," *IEEE Electron Device Lett.*, vol. 42, no. 8, pp. 1244–1247, Aug. 2021.
[18] X. Zhu and R. Gomez-Garcia, "Exploiting parasitic capacitances in 3-D inductors to design RF CMOS quasi-elliptic-type broad-band bandpass filters," *IEEE Trans. Circuits Syst. II, Exp. Briefs*, vol. 68, no. 9, pp. 3128–3132, Sep. 2021.
[19] S. K. Thapa, R. K. Pokharel, B. Chen, and A. Barakat, "On-chip millimeter-wave DGS based bandstop filter in 0.18-μm CMOS process," *IEEE Trans. Circuits Syst. II, Exp. Briefs*, vol. 69, no. 6, pp. 2732–2736, Jun. 2022.
[20] K. Song, W. Chen, S. R. Patience, Y. Chen, A. M. Iman, and Y. Fan, "Compact wide-frequency tunable filter with switchable bandpass and bandstop frequency response," *IEEE Access*, vol. 7, pp. 47503–47508, 2019.
[21] M. Jung and B.-W. Min, "A widely tunable compact bandpass filter based on a switched varactor-tuned resonator," *IEEE Access*, vol. 7, pp. 95178–95185, 2019.
[22] Y. Liu, L. Liu, C. Liang, and I. Majid, "Compact planar tunable filter with constant absolute bandwidth and wide-frequency tuning range using DGS coupling structure," *IEEE Access*, vol. 9, pp. 157259–157266, 2021.
[23] D. Jiang, Y. Liu, X. Li, G. Wang, and Z. Zheng, "Tunable microwave bandpass filters with complementary split ring resonator and liquid crystal materials," *IEEE Access*, vol. 7, pp. 126265–126272, 2019.
[24] X.-K. Bi, X. Zhang, S.-W. Wong, S.-H. Guo, and T. Yuan, "Design of notched-wideband bandpass filters with reconfigurable bandwidth based on terminated cross-shaped resonators," *IEEE Access*, vol. 8, pp. 37416–37427, 2020.
[25] K. R. Mahmoud and A. M. Montaser, "Design of compact mm-wave tunable filtenna using capacitor loaded trapezoid slots in ground plane for 5G router applications," *IEEE Access*, vol. 8, pp. 27715–27723, 2020.
[26] D. Jiang, X. Li, Z. Fu, G. Wang, Z. Zheng, T. Zhang, and W.-Q. Wang, "Millimeter-wave broadband tunable band-pass filter based on liquid crystal materials," *IEEE Access*, vol. 8, pp. 1339–1346, 2020.
[27] E. Polat, R. Reese, M. Jost, C. Schuster, M. Nickel, R. Jakoby, and H. Maune, "Tunable liquid crystal filter in nonradiative dielectric waveguide technology at 60 GHz," *IEEE Microw. Wireless Compon. Lett.*, vol. 29, no. 1, pp. 44–46, Jan. 2019.
[28] K. Y. Chan, R. Ramer, R. R. Mansour, and Y. J. Guo, "60 GHz to E-band switchable bandpass filter," *IEEE Microw. Wireless Compon. Lett.*, vol. 24, no. 8, pp. 545–547, Aug. 2014.
[29] D. Psychogiou, D. Peroulis, Y. Li, and C. Hafner, "V-band bandpass filter with continuously variable center frequency," *IET Microw., Antennas Propag.*, vol. 7, no. 8, pp. 701—707, Jun. 2013.
[30] G. Moloudian, S. Bahrami, and R. M. Hashmi, "A microstrip lowpass filter with wide tuning range and sharp roll-off response," *IEEE Trans. Circuits Syst. II, Exp. Briefs*, vol. 67, no. 12, pp. 2953–2957, Dec. 2020.
[31] S. Bahrami, G. Moloudian, H.-J. Song, and J. L. Buckley, "Reconfigurable UWB circularly polarized slot antenna with three modes of operation and continuous tuning rang," *IEEE Trans. Antennas Propag.*, vol. 70, no. 9, pp. 8542–8547, Sep. 2022.
[32] G. Shen, W. Che, and Q. Xue, "Compact microwave and millimeter-wave bandpass filters using LTCC-based hybrid lumped and distributed resonators," *IEEE Access*, vol. 7, pp. 104797–104809, 2019.
[33] M. Margalef-Rovira, A. A. Saadi, L. Vincent, S. Lepilliet, C. Gaquiere, D. Gloria, C. Durand, M. J. Barragan, E. Pistono, S. Bourdel, and P. Ferrari, "Highly tunable high-Q inversion-mode MOS varactor in the 1–325-GHz band," *IEEE Trans. Electron Devices*, vol. 67, no. 6, pp. 2263–2269, Jun. 2020.
[34] J. S. G. Hong and M. J. Lancaster, *Microstrip Filters for RF/Microwave Applications*, vol. 167. Hoboken, NJ, USA: Wiley, 2004.
[35] P. Rynkiewicz, A.-L. Franc, F. Coccetti, S. T. Wipf, M. Wietstruck, M. Kaynak, and G. Prigent, "Tunable dual-mode ring filter based on BiCMOS embedded MEMS in V-band," in *Proc. IEEE Asia Pacific Microw. Conf. (APMC)*, Nov. 2017, pp. 124–127.
[36] M. Abdelfattah, D. Psychogiou, Z. Yang, and D. Peroulis, "V-band frequency reconfigurable cavity-based bandpass filters," in *Proc. IEEE/ACES Int. Conf. Wireless Inf. Technol. Syst. (ICWITS) Appl. Comput. Electromagn. (ACES)*, Mar. 2016, pp. 1–2.
[37] H. Jiang, B. Lacroix, K. Choi, Y. Wang, A. T. Hunt, and J. Papapolymerou, "*Ka*- and *U*-band tunable bandpass filters using ferroelectric capacitors," *IEEE Trans. Microw. Theory Techn.*, vol. 59, no. 12, pp. 3068–3075, Dec. 2011.

SIROUS BAHRAMI received the M.S. and Ph.D. degrees in electrical engineering from the Iran University of Science and Technology (IUST), Tehran, Iran, in 2009 and 2014, respectively. In 2014, he joined the Department of Electrical Engineering, Salman Farsi University of Kazerun, and was involved in the investigation of tunable filters and reconfigurable antennas. He is currently a Postdoctoral Researcher with the Pohang University of Science and Technology (POSTECH), Pohang, South Korea, developing multifeed and reconfigurable antennas for RF and mm-wave communication systems. His research interests include passive and active microwave devices, planar antennas, and MMICs.

KANGSEOP LEE (Student Member, IEEE) received the B.S. and M.S. degrees in electrical engineering from the Pohang University of Science and Technology (POSTECH), Pohang, South Korea, in 2017 and 2019, respectively, where he is currently pursuing the Ph.D. degree in electrical engineering. His research interests include millimeter-waves and terahertz CMOS circuit designs.

HO-JIN SONG (Senior Member, IEEE) received the M.S. and Ph.D. degrees in electrical engineering from the Gwangju Institute of Science and Technology (GIST), Gwangju, South Korea, in 2001 and 2005, respectively. In 2006, he joined Nippon Telegraph and Telephone (NTT), Japan, where he was engaged in the development of sub-millimeter and terahertz wave devices, circuits and systems for communication, and remote sensing and imaging applications. In 2014, he was named a Distinguished Research Scientist of NTT Laboratories. Since 2016, he has been with the Department of Electrical Engineering, Pohang University of Science and Technology, Pohang, South Korea. He is currently the Director of the mm/THz Radio Research Center, established by the Ministry of Science and ICT, South Korea. His current research interests include mm-wave and terahertz circuits, antennas, packages, and test-bed systems, particularly for wireless communications, connectivity, and radar applications. He was a recipient of the GIST Best Thesis Award, in 2005, the NTT Microsystem Labs Research of the Year Award, in 2009 and 2014, the Young Scientist Award of the Spectroscopical Society of Japan, in 2010, the IEEE MICROWAVE AND WIRELESS COMPONENT LETTERS Tatsuo Itoh Best Paper Award, in 2014, and the Best Industrial Paper Award from IEEE MTTs-IMS 2016, in 2016. He was an IEEE Distinguished Microwave Lecturer, from 2019 to 2021.